One-step fabrication of nanostructures by femtosecond laser for surface-enhanced Raman scattering

Cheng-Hsiang Lin[1,2], Lan Jiang[3], Yen-Hsin Chai[4], Hai Xiao[5], Shean-Jen Chen[1], and Hai-Lung Tsai[2]*

[1]*Department of Engineering Science, National Cheng Kung University, Tainan 70101, Taiwan*
[2]*Department of Mechanical & Aerospace Engineering, Missouri University of Science and Technology, Rolla, MO USA*
[3]*Department of Mechanical and Automation Engineering, 3rd School, Beijing Institute of Technology, 100081, Beijing, China*
[4]*Department of Electrical Engineering, Technology and Science Institute of Northern Taiwan, Taipei 112, Taiwan*
[5]*Department of Electrical & Computer Engineering, Missouri University of Science and Technology, Rolla, MO, USA*
*tsai@mst.edu

Abstract: This paper reports an efficient fabrication of nanostructures on silicon substrates for surface-enhanced Raman scattering (SERS). Silicon wafer substrates in the aqueous solution of silver nitrate were machined by the femtosecond laser direct writing to achieve simultaneously in one-step the generation of grating-like nanostructures on the surface of the substrate and the formation of silver nanoparticles on the surface of the nanostructures via the laser-induced photoreduction effect. Parametric studies were conducted for the different concentrations of aqueous silver nitrate solutions and scanning speeds. The enhancement factor of the SERS is found to be higher than 10^9. The patterning technique provides an opportunity to incorporate the SERS capability in a functional microchip.

OCIS codes: (240.6695) Surface-enhanced Raman scattering; (230.3990) Micro-optical devices.

References and links

1. M. Fleischmann, P. J. Hendra, and A. J. McQuillan, "Raman spectra of pyridine adsorbed at a silver electrode," Chem. Phys. Lett. **26**(2), 163–166 (1974).
2. D. L. Jeanmaire, and R. P. Van Duyne, "Surface raman spectroelectrochemistry Part I. Heterocyclic, aromatic, and aliphatic amines adsorbed on the anodized silver electrode," J. Electroanal. Chem. **84**(1), 1–20 (1977).
3. C. Fang, A. Agarwal, K. D. Buddharaju, N. M. Khalid, S. M. Salim, E. Widjaja, M. V. Garland, N. Balasubramanian, and D. L. Kwong, "DNA detection using nanostructured SERS substrates with Rhodamine B as Raman label," Biosens. Bioelectron. **24**(2), 216–221 (2008).
4. P. Measor, L. Seballos, D. Yin, J. Z. Zhang, E. J. Lunt, A. R. Hawkins, and H. Schmidt, "On-chip surface-enhanced Raman scattering detection using integrated liquid-core waveguide," Appl. Phys. Lett. **90**(21), 211107 (2007).
5. L. Su, C. J. Rowlands, and S. R. Elliott, "Nanostructures fabricated in chalcogenide glass for use as surface-enhanced Raman scattering substrates," Opt. Lett. **34**(11), 1645–1647 (2009).
6. K. Kneipp, Y. Wang, H. Kneipp, L. T. Perelman, I. Itzkan, R. R. Dasari, and M. S. Feld, "Single Molecule Detection Using Surface-Enhanced Raman Scattering (SERS)," Phys. Rev. Lett. **78**(9), 1667–1670 (1997).
7. R. J. C. Brown, and J. T. Milton, "Nanostructures and nanostructured substrates for surface-enhanced Raman scattering (SERS)," J. Raman Spectrosc. **39**(10), 1313–1326 (2008).
8. P. C. Lee, and D. Meisel, "Adsorption and surface-enhanced Raman of dyes on silver and gold sols," J. Phys. Chem. **86**(17), 3391–3395 (1982).
9. H. Hada, Y. Yonezawa, A. Yoshida, and A. Kurakake, "Photoreduction of silver ion aqueous and alcoholic solutions," J. Phys. Chem. **80**(25), 2728–2731 (1976).
10. R. Sato-Berrú, R. Redón, A. Vázquez-Olmos, and J. M. Saniger, "Silver nanoparticles synthesized by direct photoreduction of metal salts. Application in surface-enhanced Raman spectroscopy," J. Raman Spectrosc. **40**(4), 376–380 (2009).
11. X. Tian, K. Chen, and G. Cao, "Seedless, surfactantless photoreduction synthesis of silver nanoplates," Mater. Lett. **60**(6), 828–830 (2006).
12. H. T. Tung, I. G. Chen, J. M. Song, and C. W. Yen, "Thermally assisted photoreduction of vertical silver nanowires," J. Mater. Chem. **19**(16), 2386–2391 (2009).

#117604 - $15.00 USD Received 22 Sep 2009; revised 6 Nov 2009; accepted 6 Nov 2009; published 11 Nov 2009

13. Z. Zhou, J. Xu, Y. Cheng, Z. Xu, K. Sugioka, and K. Midorikawa, "Surface-enhanced Raman scattering substrate fabricated by femtosecond laser direct writing," Jpn. J. Appl. Phys. **47**(1), 189–192 (2008).
14. S. Maruo, and T. Saeki, "Femtosecond laser direct writing of metallic microstructures by photoreduction of silver nitrate in a polymer matrix," Opt. Express **16**(2), 1174–1179 (2008).
15. A. Ishikawa, T. Tanaka, and S. Kawata, "Improvement in the reduction of silver ions in aqueous solution using two-photon sensitive dye," Appl. Phys. Lett. **89**(11), 113102 (2006).
16. S. J. Henley, and S. R. P. Silva, "Laser direct write of silver nanoparticles from solution onto glass substrates for surface-enhanced Raman spectroscopy," Appl. Phys. Lett. **91**(2), 023107 (2007).
17. R. R. Gattass, and E. Mazur, "Femtosecond laser micromachining in transparent material," Nat. Photonics **2**(4), 219–225 (2008).
18. T. Wei, Y. Han, H. L. Tsai, and H. Xiao, "Miniaturized fiber inline Fabry-Perot interferometer fabricated with a femtosecond laser," Opt. Lett. **33**(6), 536–538 (2008).
19. C. H. Lin, L. Jiang, H. Xiao, Y. H. Chai, S. J. Chen, and H. L. Tsai, "Fabry-Perot interferometer embedded in a glass chip fabricated by femtosecond laser," Opt. Lett. **34**(16), 2408–2410 (2009).
20. J. Bonse, S. Baudach, J. Krüger, W. Kautek, and M. Lenzner, "Femtosecond laser ablation of silicon-modification thresholds and morphology," Appl. Phys., A Mater. Sci. Process. **74**(1), 19–25 (2002).
21. C. H. Crouch, J. E. Carey, M. Shen, E. Mazur, and F. Y. Genin, "Infrared absorption by sulfur-doped silicon formed by femtosecond laser irradiation," Appl. Phys., A Mater. Sci. Process. **79**, 1635–1641 (2004).
22. Z. Huang, J. E. Carey, M. Liu, X. Guo, E. Mazur, and J. C. Campbell, "Microstructured silicon photodetector," Appl. Phys. Lett. **89**(3), 033506 (2006).
23. E. D. Diebold, N. H. Mack, S. K. Doorn, and E. Mazur, "Femtosecond laser-nanostructured substrates for surface-enhanced Raman scattering," Langmuir **25**(3), 1790–1794 (2009).
24. M. Futamata, and Y. Maruyama, "Electromagnetic and chemical interaction between Ag nanoparticles and adsorbed rhodamine molecules in surface-enhanced Raman scattering," Anal. Bioanal. Chem. **388**(1), 89–102 (2007).
25. Y. Han, C. H. Lin, H. Xiao, and H. L. Tsai, "Femtosecond laser-induced silicon surface morphology in water confinement," Microsyst. Technol. **15**(7), 1045–1049 (2009).
26. T. Kondo, K. Nishio, and H. Masuda, "Surface-enhanced Raman scattering in multilayered Au nanoparticles in anodic porous alumina matrix," Appl. Phys. Express **2**, 032001 (2009).
27. I. W. Sztainbuch, "The effects of Au aggregate morphology on surface-enhanced Raman scattering enhancement," J. Chem. Phys. **125**(12), 124707 (2006).
28. P. A. Temple, and C. E. Hathaway, "Multiphonon Raman spectrum of silicon," Phys. Rev. B **7**(8), 3685–3697 (1973).
29. R. P. Van Duyne, J. C. Hulteen, and D. A. Treichel, "Atomic force microscopy and surface-enhanced Raman spectroscopy. 1. Ag island films and Ag film over polymer nanosphere surface supported on glass," J. Chem. Phys. **99**(3), 2101–2115 (1993).
30. G. L. Liu, and L. P. Lee, "Nanowell surface enhanced Raman scattering arrays fabricated by soft-lithography for label-free biomolecular detections in integrated microfluidics," Appl. Phys. Lett. **87**(7), 074101 (2005).

1. Introduction

Since the surface-enhanced Raman scattering (SERS) was discovered [1,2], it has been widely employed for molecular detection due to its capabilities of providing simultaneously the structural [3] and quantitative information [4,5] as well as strong signal enhancements up to 10^{14} for single molecular detections [6]. The strength of enhancement depends on the exciting wavelength and properties of the metal nanostructures which affect the interaction between the electromagnetic (EM) field and the nanostructures when plasmon propagates at their surfaces. Since the enhancement factors (EFs) depend on the properties of the metal nanostructures, such as the surface morphology, categories of metals, and chemical environment of the nanostructures, a variety of approaches have been developed to fabricate SERS substrates for high EFs, including the electrochemically roughened electrodes, aggregates of colloidal gold or silver particles, and nanolithography [7].

Metal nanocomponents can be synthesized by chemical-reduction [8] or photoreduction [9] from metal salts into different types of formations such as nanoparticles [10], nanoplates [11], and nanowires [12]. Employing the photoreduction mechanism to synthesize metal particles has been demonstrated in glass [13], polymer matrix [14] and solutions [10]. SERS measurements can be conducted directly in the produced metal colloids or on the solid substrates immobilized with synthesized metal nanoparticles by chemical methods or directly on the deposited nanoparticles by physical methods. The photoreduction process produces metal colloids as well as 2D or 3D microstructures on a solid support [15]. The light source used to reduce metal cations can be a lamp-based white light [10], a nanosecond laser [16], or a femtosecond (fs) laser [14,15].

#117604 - $15.00 USD Received 22 Sep 2009; revised 6 Nov 2009; accepted 6 Nov 2009; published 11 Nov 2009

Fs laser micromachining has attracted much attention due to the unique properties of minimum thermal damage as the pulse duration is shorter than the thermalization time, and the phenomenon of multiphoton absorption leading to the benefit of machining dielectrics inside the bulk material [17]. Fs laser micromachining in dielectric materials opens a window of opportunity to fabricate functional microdevices directly [18] or indirectly [19]. Recently, periodic micro/nano-structures generated by fs laser irradiations on silicon wafers were demonstrated [20]. Their unique optical property of high absorbability in a wide range of wavelengths (visible light to IR) can be very important for optical detectors to enhance the optical-electric efficiency and the effective wavelength range [21,22]. Furthermore, the periodic surface morphology, after depositing metal particles on the surface, was used as the SERS substrate [23].

In this work, we develop an efficient approach to fabricate SERS substrates which provide high EFs. A combined process of material ablation, particle synthesis, and particle deposition were achieved by fs laser micromachining of silicon wafers in aqueous solutions of silver nitrate. A high EF of 10^9 was obtained for the synthesized silver nanoparticles on the substrate using Rhodamine 6G (R6G) as analyte molecules at the excitation wavelength of 632.8 nm.

2. Experimental procedures

2.1 Femtosecond laser micromachining system

The fs laser micromachining system used in this study consists of an amplified fs laser (Legend-F, Coherent), a computer controlled five-axis motion stage (Areoteck) with a resolution of 1 μm, and an in-line imaging system to monitor the machining process. The central wavelength, maximum repetition rate, and pulse width of the fs laser are, respectively, 800 nm, 1 kHz, and 120 fs. The maximum average output power is 1 W which corresponds to the pulse energy of 1 mJ. The working pulse energy is adjusted by a combination of a half-wave plate and a linear polarizer to meet different experimental requirements.

2.2 Sample preparation

Silicon wafer substrates were cleaned in an ultrasonic bath with acetone for 10 minutes and then rinsed by de-ionized water. The cleaned substrates were dipped into 2 ml diluted aqueous solutions of silver nitrate with different concentrations from 1 M to 1 mM contained in an open plastic vessel. The fs laser pulses were focused onto the sample via a 10 × objective lens (NA = 0.3) with a spot size of about 3.3 μm and the samples were translated by the motion stage during the line-by-line machining process. The pulse energy was adjusted to 27 nJ which corresponds to about 0.3 J/cm^2. The scanning pitch was set as 1 μm and the scanning speed was varied from 0.5 mm/min to 10 mm/min which correspond to the number of laser pulses deposited on a unit area (NLPDUA) from about 400 to 20. Note for the scanning speed V (with the unit of mm/min), the NLPDUA = (60 × 3.3) / V, where 3.3 is the laser spot size with the unit of μm. After the machining process, the samples were rinsed in de-ionized water to clean up the excess silver nitrate solution. The morphology and composition of the produced nanostructures were examined using scanning electron microscopy (SEM) and energy dispersed spectrum (EDS) respectively.

2.3 SERS measurement

In the SERS measurement, the aqueous solution of R6G with concentrations of 10^{-3} M and 10^{-7} M added with 10 mM of sodium chloride were utilized to calibrate the EFs. The Cl^- anions of sodium chloride were used to stabilize the adsorbent on the silver particles and to induce the electronic interaction between them [24]. The machined samples were dipped into analyte solutions keeping a 1 mm thick liquid layer above the sample surface and held 30 min for incubation. The SERS measurements were performed by means of a commercial Ramanscope (Jobin Yvon) integrated with an upright microscope using a He-Ne laser as a light source with 632.8 nm wavelength. The maximum exciting power is 17 mW. The

#117604 - $15.00 USD Received 22 Sep 2009; revised 6 Nov 2009; accepted 6 Nov 2009; published 11 Nov 2009

employed exciting power and the signal accumulation time are adjustable. The objective lens and grating used in this work were, respectively, 10 × (NA = 0.25) and 600 line/mm.

3. Results and discussion

3.1 Evaluation of nanostructures

First, the silicon wafer was machined by fs laser pulses in de-ionized water at different scanning speeds and the resulting surface morphology images are illustrated in Fig. 1. It is seen, at high scanning speeds, 10 mm/min [Fig. 1(a)] and 5 mm/min [Fig. 1(b)], the morphology of the roughened surface seems rather random. At the scanning speed of 2 mm/min [Fig. 1(c)], the grating-like periodic nanostructures start to appear but they are not completely developed. At high scanning speeds, 1 mm/min and 0.5 mm/min, the nanostructures have been completely developed and the period is independent of the scanning speed. The existence of grating-like nanostructures with a submicron period agrees with the previous studies [20]. Compared with the period of the structures machined in air, the structure period machined in water is smaller which reveals a smoother surface in the large scale [25]. Besides the grating-like structures, no apparent nanoparticle is observed in this case of machining in de-ionized water.

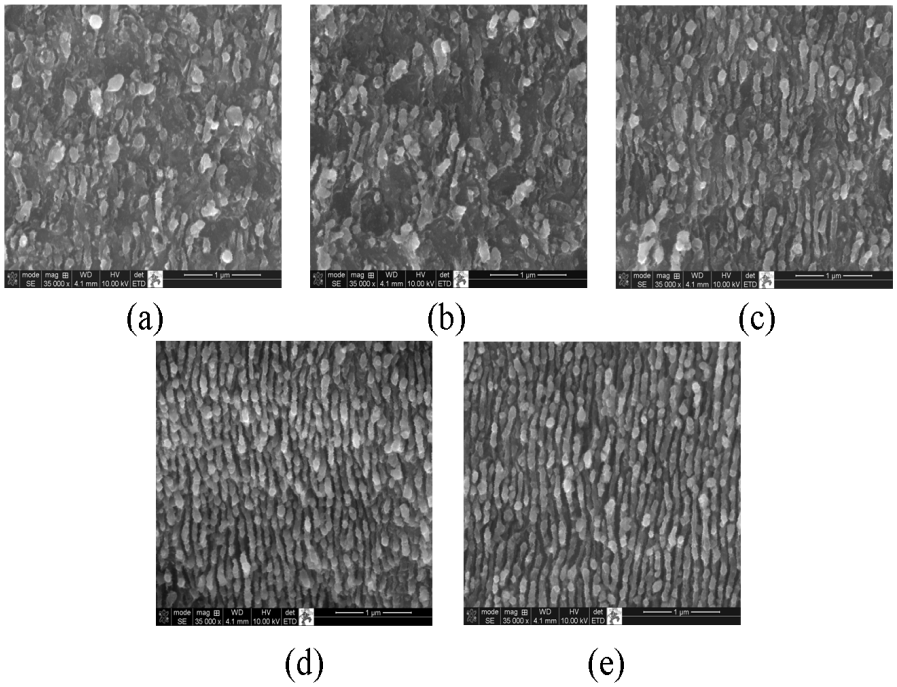

Fig. 1. Surface morphologies of the machined silicon wafer substrates in de-ionized water with scanning speeds of (a) 10 mm/min, (b) 5 mm/min, (c) 2 mm/min, (d) 1 mm/min, and (e) 0.5 mm/min.

Figure 2 shows the surface morphologies of silicon substrates machined in 0.1 M aqueous solutions of silver nitrate at different scanning speeds ranging from 10 mm/min to 0.5 mm/min. When the sample was machined in the aqueous solutions of silver nitrate with different scanning speeds, nanoparticles attached to the machined surface are clearly seen as compared to Fig. 1. The number of attached nanoparticles increases with the decreasing of scanning speed (increasing of NLPDUA). In Fig. 2(a) and 2(b), the periodic structures are not fully developed yet due to the high scanning speeds (low NLPDUA) and only a few nanoparticles on the surface can be seen. In Fig. 2(c) to 1(e), the particle density significantly

#117604 - $15.00 USD Received 22 Sep 2009; revised 6 Nov 2009; accepted 6 Nov 2009; published 11 Nov 2009

increases once the scanning speed is slower than 2 mm/min (NLPDUA = 100). In order to identify the compositions of the nanoparticles, the EDS chemical composition mapping was taken as shown in Fig. 3. Figure 3(a) reveals the mapping area and Fig. 3(b) and Fig. 3(c) show, respectively, the silver mapping and silicon mapping. The composition of the deposited nanoparticles was proven to be silver. The particle size ranges from tens of nm to hundreds of nm which is evaluated from the enlarged SEM images. From the SEM images, the synthesized nanoparticles reside on the machined surface as well as on the valleys of the grating-like nanostructures. The nanoparticles in the valleys form multilayer nanoparticle clusters similar to those published before [26], which leads to higher EFs as compared to single layer structures. Furthermore, the format of nanoparticles on the machined surface appears to be particle aggregations. These aggregation structures are also proven to cause higher EFs [27] due to the creation of "hot spots" with strong EM field enhancements in the nanogap between particles in the aggregations.

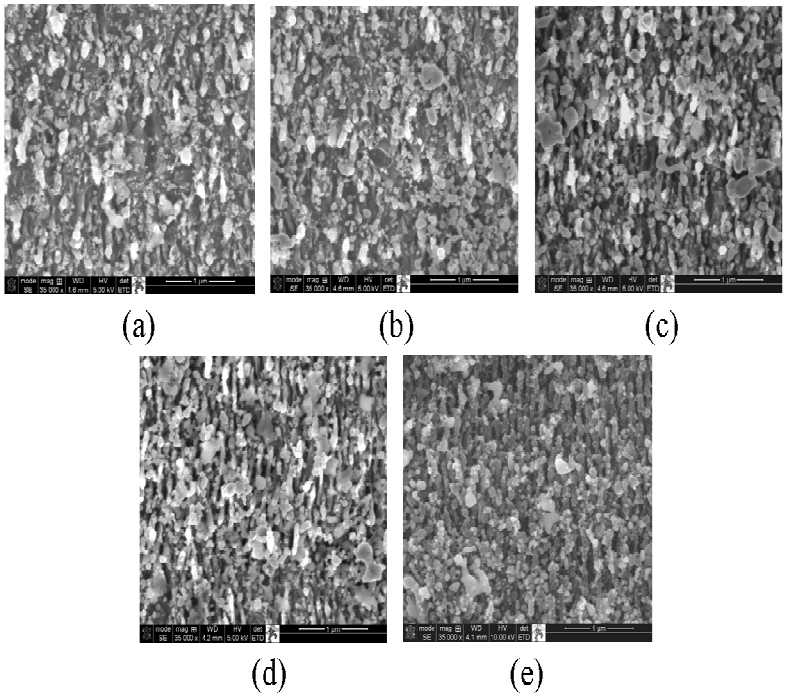

Fig. 2. Surface morphologies of the machined silicon wafer substrates in 0.1 M silver nitrate solutions with different scanning speeds. (a) 10 mm/min. (b) 5 mm/min. (c) 2 mm/min. (d) 1 mm/min. (e) 0.5 mm/min.

#117604 - $15.00 USD Received 22 Sep 2009; revised 6 Nov 2009; accepted 6 Nov 2009; published 11 Nov 2009

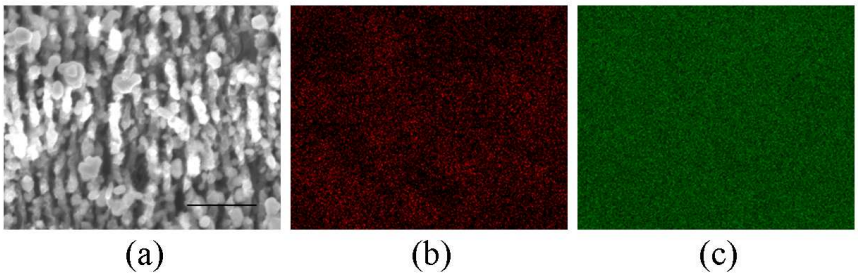

Fig. 3. EDS mapping of the sample machined in 0.1 M silver nitrate solutions at a scanning speed of 1 mm/min. (a) SEM image of the mapping area. The scale bar is 500 nm. (b) silver mapping. (c) silicon mapping.

Figure 4 shows the surface morphologies of the machined silicon wafer substrates in 1 mM, 10 mM, 0.1 M, and 1 M silver nitrate solutions with the same scanning speed of 0.5 mm/min. For low concentration, 1 mM [Fig. 4(a)], silver particles are still being developed and the particle density attached to the nanostructure is relative low. When the concentration of the silver nitrate solution increases, the particle density increases as Fig. 4(b). However, there is not much difference in particle density between 0.1 M [Fig. 4(c)] and 1 M [Fig. 4(d)]. In other words, the particle density appears to reach saturation when the concentration is higher than 0.1 M.

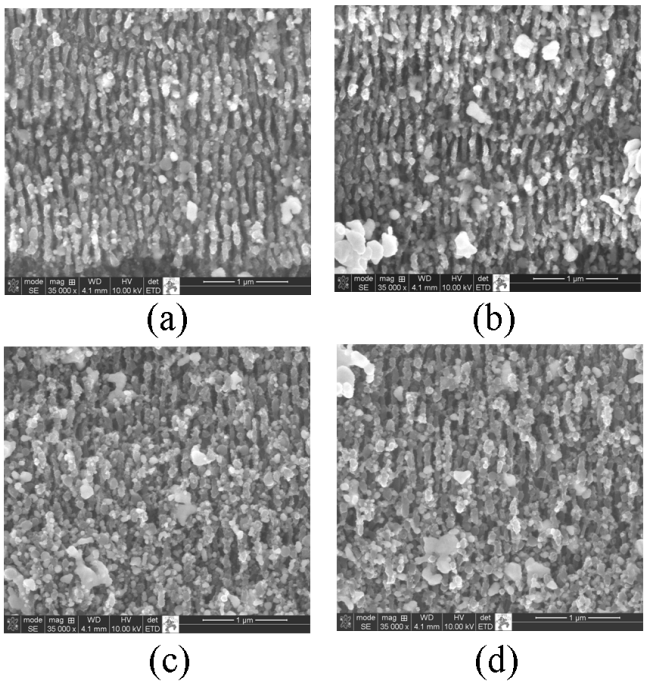

Fig. 4. Surface morphologies of the machined silicon wafer substrates in different concentrations of silver nitrate solutions with a scanning speed of 0.5 mm/min. (a) 1 mM. (b) 10 mM. (c) 0.1 M. (d) 1 M.

3.2 Parametric study

The fs laser pulse energy has dual functions; one is to ablate the substrate to become grating-like nanostructures and the other is to reduce the Ag^{+} cations in the silver nitrate solution to Ag atoms by photoreduction mechanism [9] which will attach to the nanostructures. Hence,

#117604 - $15.00 USD Received 22 Sep 2009; revised 6 Nov 2009; accepted 6 Nov 2009; published 11 Nov 2009

the entire process is a combination of material ablation and the subsequent photoreduction and particle deposition. Apparently, the laser energy density must be greater than the damage threshold of the substrate in order to ablate it. The first several laser pulses will ablate the material until the ablation is saturated, i.e., no additional ablation occurs, then, the subsequent laser pulses will produce silver nanoparticles. Before the ablation saturation is reached, some nanoparticles may be produced, they would be ablated by the subsequent laser pulses. Figure 5 illustrates the relation of SERS intensity (610 cm^{-1}) and NLPDUA at various concentrations of silver nitrate solutions. In the low concentrations (1 mM and 10 mM), the increase of NLPDUA does not lead to an apparent increase of SERS intensity. Hence, a higher concentration of silver nitrate solutions is required to increase the population of nanoparticles. As it takes time to photoreduce the Ag^{+} cations, the laser scanning speed must be slow enough (i.e., the NLPDUA must be high enough) allowing time for the photoreduction to occur and for the formation of nanoparticles. As shown in Fig. 5, for the concentration at 0.1 M, the high scanning speeds at 10 mm/min and 5 mm/min, which correspond, respectively, to 20 and 40 of NLPDUA, the SERS intensities are relative low. This is because there is not enough time for the formation of nanoparticles. In contrast, if the scanning speed is below 2 mm/min (NLPDUA = 100), the SERS intensity arises significantly. Hence, there exists a threshold scanning speed which depends on the concentration of the solution and the laser pulse energy to generate nanoparticles. For the 1 M concentration of silver nitrate solutions, the scanning speed has to be below 1 mm/min to observe the apparent signal enhancement. During the machining process in the 1 M silver nitrate solutions, it was observed that a large amount of reduced silver particles in the solution causes the solution to become locally semi-opaque. As a result, the fs laser pulse energy would be scattered or absorbed by the dense particles in the solution reducing the effective fluence to arrive at the substrate surface and, thus, more laser pulses are required to achieve the ablation saturation and to generate nanoparticles on the surface of the nanostructures which leads to the lag of SERS intensity increase at 1 mm/min. Note the SERS intensities for 0.1 M and 1 M at NLPDUA = 400 are very close to each other which is consistent with the discussion in Fig. 4 that their surface morphologies are very similar and the nanoparticle density has reached saturation at 0.1 M.

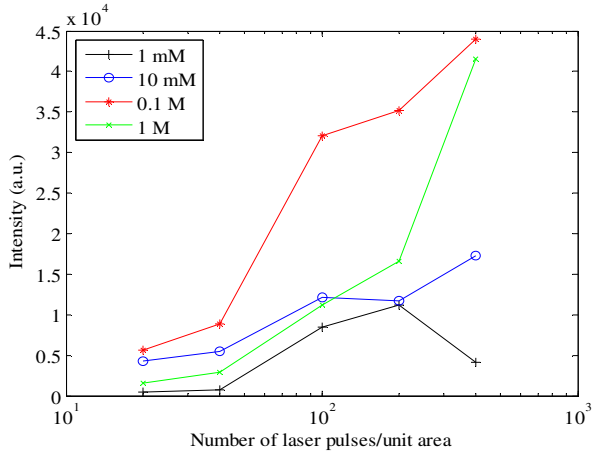

Fig. 5. SERS intensity vs. NLPDUA in different concentrations of silver nitrate solutions.

3.3 Estimation of enhancement factor

The black line and blue line in Fig. 6 show, respectively, the measured SERS spectra of 10^{-7} M R6G in the area inside (black) and outside (blue) of the machined region in the 0.1 M silver nitrate solutions. It is seen the SERS spectra in the machined area is very strong, while it is almost zero outside of the machined area. The strong signal enhancement by the deposited silver nanoparticles is evident. The red line and green line in Fig. 6 show, respectively, the

#117604 - $15.00 USD Received 22 Sep 2009; revised 6 Nov 2009; accepted 6 Nov 2009; published 11 Nov 2009

normal Raman spectra of 10^{-3} M R6G on the sample machined in de-ionized water (red) and its magnified spectrum (green). For SERS and normal Raman spectra, the exciting He-Ne laser powers are, respectively, 0.17 mW and 17 mW, and the accumulating times are, respectively, 0.5 s, 10 s. In the normal Raman spectrum of 10^{-3} M R6G on the sample machined in de-ionized water, weak R6G signals are seen in the magnified spectrum (green line), except a strong sharp peak at 520 cm^{-1} and a broad peak from 950 cm^{-1} to 1000 cm^{-1}. The results indicate the silicon substrate is observed due to the high exciting laser power and long accumulating time [28]. However, the signal of silicon is unapparent in the SERS spectra due to the existence of strong signal enhancement in the adsorbent R6G molecules which is several orders of magnitude greater than the Raman signal of silicon. In order to quantify the performance of the SERS substrate, the SERS signals of 10^{-7} M R6G measured on the sample that was machined in the 0.1 M silver nitrate solution are compared to the normal Raman signals of 10^{-3} M R6G measured on the sample that was machined in de-ionized water. Both samples were machined at the same scanning speed of 1 mm/min. The commonly accepted EF is defined by the following equation:

$$EF = \frac{I_{SERS}}{N_{SERS}} / \frac{I_{nR}}{N_{nR}} \tag{1}$$

where I_{nR} and I_{SERS} are, respectively, the intensities of normal Raman and SERS in the unit of $mW^{-1}s^{-1}$ [29]. N_{nR} and N_{SERS} represent, respectively, the number of molecules probed in the reference sample and on the SERS substrate. Due to rough surface morphology of the nanostructures with and without silver nanoparticles, the number of adsorbent molecules is difficult to measure accurately. Thus, two comparable samples were machined, respectively, in water and in the silver nitrate solution to generate the same (or very similar) surface roughness. Assuming the effective surface areas of both nanostructures are identical and there is no specific binding between the analyte and the sample surface, the number of adsorbent molecules on the surface is proportional to the concentration of the analyte solution in which the sample was dipped [30]. Using Eq. (1) and the aforementioned assumptions and conditions, the EFs at Raman peaks 610 cm^{-1}, 1310 cm^{-1}, 1360 cm^{-1}, and 1510 cm^{-1} are, respectively, 1.3×10^9, 1.1×10^9, 1.3×10^9 and 1.7×10^9, which demonstrates the high sensitivity for SERS measurements with a low R6G concentration.

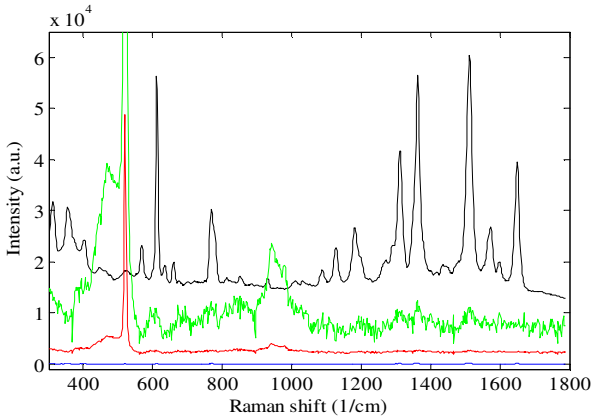

Fig. 6. SERS and Raman spectra. Black: SERS spectrum of 10^{-7} M R6G measured in the area machined by fs laser in the 0.1 M silver nitrate solution. blue: SERS spectrum of 10^{-7} M R6G measured in the un-machined area. red: Raman spectrum of 10^{-3} M R6G measured in the area machined by fs laser in the de-ionized water. green: magnified (10 ×) Raman spectrum of 10^{-3} M R6G measured in the area machined by fs laser in the de-ionized water.

#117604 - $15.00 USD Received 22 Sep 2009; revised 6 Nov 2009; accepted 6 Nov 2009; published 11 Nov 2009

4. Conclusions

By fs laser machining of silicon wafer in the aqueous solutions of silver nitric under a suitable concentration and laser scanning speed, the generation of grating-like nanostructures and the subsequent formation of silver nanoparticles on the nanostructures were simultaneously accomplished. The one-step fabrication of SERS substrates with high enhancement factors of 10^9 was demonstrated. The selective laser patterning approach provides the opportunity of directly fabricating SERS active substrates in a functional micro device or chip.

Acknowledgments

This work was supported by the U.S. Department of Energy under Contract No. DE-FE0001127 and the 111 project of China under Grant No. B08043.

#117604 - $15.00 USD Received 22 Sep 2009; revised 6 Nov 2009; accepted 6 Nov 2009; published 11 Nov 2009